Crucial role of nuclear dynamics for electron injection in a dye-semiconductor Complex

Monti, A.; Negre, C.F.A.; Batista, V.S.; Rego, L.G.C.; Groot, H.J.M. de; Buda, F.

THE JOURNAL OF PHYSICAL CHEMISTRY Letters

Letter

pubs.acs.org/JPCL

Crucial Role of Nuclear Dynamics for Electron Injection in a Dye–Semiconductor Complex

Adriano Monti,[†] Christian F. A. Negre,[§] Victor S. Batista,[‡] Luis G. C. Rego,[∥] Huub J. M. de Groot,[†] and Francesco Buda*,[†]

[†]Leiden Institute of Chemistry, Leiden University, Einsteinweg 55, 2300 RA, Leiden, The Netherlands

[‡]Department of Chemistry, Yale University, P.O. Box 208107, New Haven, Connecticut 06520, United States

[§]Theoretical Division, Los Alamos National Laboratory, P.O. Box 1663, Los Alamos, New Mexico 87545, United States

[∥]Department of Physics, Universidade Federal de Santa Catarina, Florianópolis, Santa Catarina 88040-900, Brazil

Supporting Information

ABSTRACT: We investigate the electron injection from a terrylene-based chromophore to the TiO_2 semiconductor bridged by a recently proposed phenyl-amide-phenyl molecular rectifier. The mechanism of electron transfer is studied by means of quantum dynamics simulations using an extended Hückel Hamiltonian. It is found that the inclusion of the nuclear motion is necessary to observe the photoinduced electron transfer. In particular, the fluctuations of the dihedral angle between the terrylene and the phenyl ring modulate the localization and thus the electronic coupling between the donor and acceptor states involved in the injection process. The electron propagation shows characteristic oscillatory features that correlate with interatomic distance fluctuations in the bridge, which are associated with the vibrational modes driving the process. The understanding of such effects is important for the design of functional dyes with optimal injection and rectification properties.

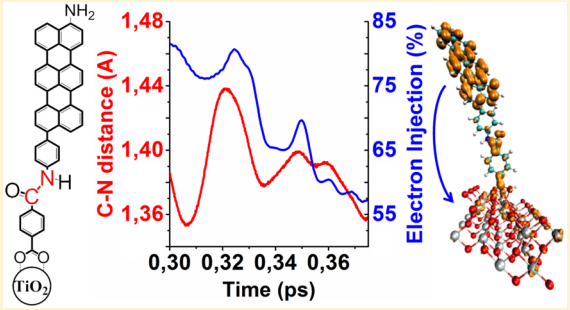

Environmentally friendly and cost-effective dye-sensitized solar cells (DSSCs) are a potential alternative to silicon-based photovoltaics for solar energy conversion, can be equipped with molecular catalysts for direct conversion and storage of solar energy into fuel, and have been the subject of extensive research.[1−5] In DSSC devices a semiconductor electrode is functionalized with a (molecular) chromophore absorbing visible light. The photoexcitation induces an interfacial electron transfer (ET) from the dye into the semiconductor conduction band (CB), while an electrolyte shuttles electrons from the counter electrode to regenerate the oxidized dye.

Despite considerable improvement achieved in recent years, DSSC performances have not reached energy conversion yield and efficiency levels that are necessary to render them competitive with silicon-based solar cells. Higher efficiencies can be attained by increasing the light-harvesting properties of the solar cell, by decreasing internal energy losses, or by optimizing the conditions for fast electron injection.

A major obstacle hampering the performance of DSSC devices is the internal losses from recombination between the electron injected into the semiconductor and the hole on the oxidized dye.[6] In an effort to design more efficient devices, several groups have investigated the effect of specific cell parameters for enhancing electron injection and reducing recombination losses, such as the length and nature of the bridges,[7−10] the chemical structure of the anchor groups[11] and the redox potential of the electrolyte.[12] In addition, detailed investigations of the molecular mechanisms at the dye/semiconductor interface[13−18] have revealed the importance of nonadiabatic dynamics for charge separation and recombination.[19−21]

In an approach to prevent back electron transfer, Batista and coworkers recently proposed the use of a molecular rectifier[22] composed of two phenyl rings coupled through an amide bond (see AM molecule in Scheme 1a). This molecule acts as a rectifier when used as a molecular wire or as a linker-chromophore in a solar cell device.[23,24] Used as a molecular bridge between a dye and a semiconductor, a rectifying AM linker could increase the DSSC efficiency by decreasing the electron−hole recombination rate.

To investigate the role of AM in the electron injection process, we use it to bridge an amine-functionalized terrylene antenna (T) and a titanium dioxide (TiO_2) anatase surface (T-AM-TiO_2, Scheme 1b). Terrylene is a well-characterized molecule that absorbs within the visible spectrum (∼580 nm) and has an excited-state lifetime on the nanosecond time scale.[25,26] Recently this molecule has been also used as an

Received: April 28, 2015
Accepted: June 5, 2015
Published: June 5, 2015

DOI: 10.1021/acs.jpclett.5b00876
J. Phys. Chem. Lett. 2015, 6, 2393−2398

Scheme 1. Chemical Structure of the Molecular Rectifier AM (a) and of the T-AM Dye (b)[a]

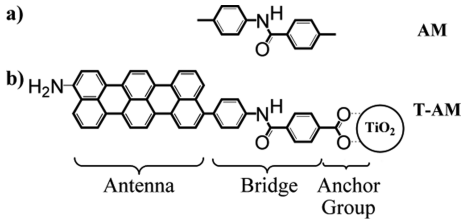

[a]Anchoring of the chromophore to the TiO_2 semiconductor through a carboxylic acid group (anchor group) leads to the formation of the T-AM-TiO_2 system.

electron donor for TiO_2-based DSSC.[27] TiO_2, in turn, is a semiconductor material widely used as an electron collector in DSSC and is known for its stability and favorable electronic properties.[6] The anchoring of the dye onto TiO_2 is achieved through a carboxylic acid group in a bidentate bridging mode (Scheme 1b).

To provide insights for the design of more efficient charge separators, we investigate the quantum dynamics of electron injection coupled to thermal nuclear motion. We show that the nuclear dynamics opens an electron injection channel in the T-AM-TiO_2 system by a coherent superposition of states. The conversion of the initial excited state on the chromophore into a charge-transfer state between the chromophore and the TiO_2 is driven by normal modes localized at the interface between the antenna and the semiconductor. Our results support recent findings on the importance of coherent vibronic coupling during photoinduced charge separation processes for both natural and artificial light-harvesting systems.[16,28−34]

The electron quantum dynamics (EQD) simulations are performed using a tight-binding model Hamiltonian based on the extended Hückel (EH) method,[35] which is parametrized against DFT/B3LYP[36,37] results (see also SI-1 in the Supporting Information). At the beginning of each quantum dynamics simulation, the photoexcited electron and the photoinduced hole wavepackets are initialized as the lowest unoccupied (LUMO) and highest occupied molecular orbitals (HOMO) of the isolated chromophore T-AM (see Table S2, Supporting Information). In this way we ensure that the initial wavepackets are not stationary states of the entire T-AM-TiO_2 system. Following the method described by Rego and coworkers to study intramolecular and interfacial ET processes,[38,39] the quantum propagation of the wavepackets is performed both for fixed molecular geometries and over classical nuclear trajectories obtained beforehand with the ab initio molecular dynamics (MD) approach implemented in the CPMD program.[40] Hence, the nuclear trajectories are calculated separately from the dynamics of the electronic wavepacket. This is justified because we are interested in the response of the electronic quantum system to the thermal nuclear motion. The electron quantum dynamics as well as the ab initio MD are performed with a time step of 0.1 fs. A detailed description of the method, the parametrization procedure, and the computational setup are reported in the Supporting Information (SI-1 and SI-2).

In Figure 1, the total densities of the unoccupied states of the T-AM-TiO_2 system projected on the chromophore (dye, in blue) and on the semiconductor (TiO_2, in gray) are compared. To prepare the system, we employed the T-AM structure for

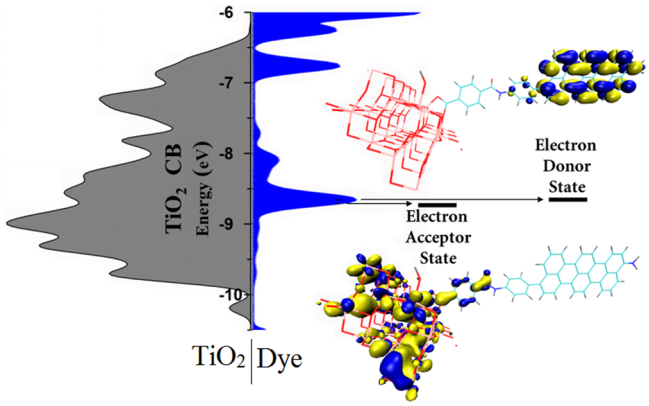

Figure 1. Comparison between the density of the chromophore unoccupied states (Dye, in blue) and of the TiO_2 conduction band (TiO_2, in gray). The calculations are performed for the entire T-AM-TiO_2 system. On the right-hand side, the electron donor and acceptor states contributing to the peak around −8.7 eV are represented.

the parametrization of the EH Hamiltonian (see SI-1). The projected density of states (DOS) of T-AM (Figure 1, dye) presents a peak at −8.7 eV. This peak is associated with the two almost degenerate ($\Delta\varepsilon$ = −0.05 eV) unoccupied system orbitals shown in Figure 1. These two orbitals, labeled electron donor (ED) and electron acceptor (EA) states, correspond, respectively, to the LUMO and LUMO+1 of the isolated dye molecule (Table S2 of Supporting Information).

An EQD simulation is performed for the T-AM-TiO_2 system over the same set of nuclear coordinates used for the DOS calculation, keeping the nuclear positions fixed. Because the photoexcitation of the dye populates the molecular orbital localized on the terrylene (ED), the photoexcited electron has to travel across the bridge through the EA state to reach the TiO_2 surface. Despite the proximity between the electron donor and acceptor states and the presence of a thermodynamic driving force, no ET from T-AM to TiO_2 is observed within the 2 ps EQD simulation in the absence of nuclear motion (see Figure S2 in the Supporting Information).

To investigate the effect of the nuclear motion on the electron dynamics, we repeated the hole/electron quantum dynamics calculations by evolving the wavepackets over a classical MD trajectory obtained beforehand (see SI-2).[41,42] Because we use a nuclear trajectory obtained in the ground state, the effect of the thermal relaxation of the photogenerated hot exciton is not included; however, because this effect is fast and highly localized on the antenna, it is not expected to significantly affect the dynamics of the ET on a longer time scale[6] (see also Supporting Information SI-3). The results of the electron quantum dynamics performed along the MD trajectory are reported in Figure 2, showing the survival probability (SP) of the electron wavepacket. The SP is defined as the time-dependent population of the wavepacket within the dye:[39] SP = 1 when the wavepacket is fully localized within the sensitizer, while SP = 0 when it is fully transferred to TiO_2.

The survival probability profile (Figure 2, SP) shows that the introduction of nuclear dynamics induces significant ET within the first few hundreds femtoseconds, in contrast with the results for the T-AM-TiO_2 without nuclear dynamics (Figure S2 in the Supporting Information). This demonstrates the importance of the coupling between the electron dynamics and thermal motions in the description of ET processes.

DOI: 10.1021/acs.jpclett.5b00876
J. Phys. Chem. Lett. 2015, 6, 2393−2398

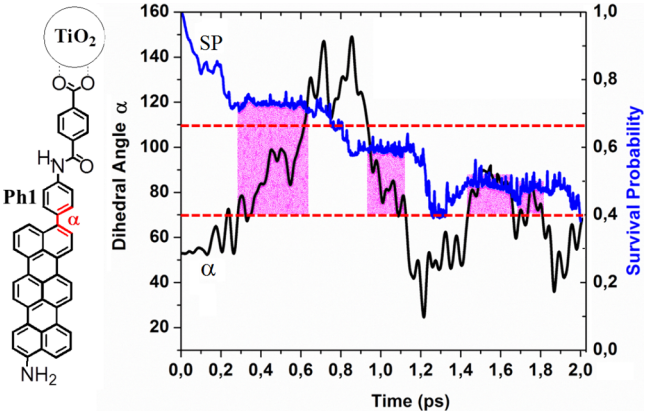

Figure 2. Electron quantum dynamics simulation of the T-AM-TiO_2 system (SP, blue) along a classic MD trajectory obtained with CPMD. The electron and nuclear dynamics both employ a time step $\delta\tau$ = 0.1 fs. A schematic representation of the analyzed complex is presented on the left-hand side of the Figure, together with the identification of the dihedral angle α (in red). The black line (α) represents the variation of this angle along the dynamics. The range of values identified as crucial for electron injection is delimited by the red dashed lines. The regions highlighted in pink correspond to time intervals in which the dihedral angle α falls within this range.

Additionally, the SP profile is characterized by the presence of plateaus emerging periodically every ~250 fs, indicating that the electron injection is temporarily quenched. At the same time the SP evolution shows that back charge transfer from the semiconductor on the terrylene antenna does not occur. This behavior can be associated with the rectification property of the AM bridge (see Supporting Information SI-4). The analysis of the molecular dynamics trajectory reveals a correlation between the recurrence of these plateaus and the fluctuation of the dihedral angle α (Figure 2, α), defined between the terrylene and the phenyl ring Ph1 (see Figure 2, left). The electron injection occurs only when α presents a value <70° or >110° (red dashed lines). On the contrary, if α is comprised within these two values, the transfer is hindered (areas highlighted in pink, Figure 2). The variation of the dihedral angle α influences the delocalization of the electron donor state over the Ph1 ring, as shown in Figure S3 (Supporting Information). When 70° < α < 110°, the ED state is confined on the antenna (T) and is separated from the electron acceptor orbital by the Ph1 ring; however, when α is outside the aforementioned range, the planarity and consequently the conjugation between Ph1 and the terrylene is increased. This induces the delocalization of the ED state over Ph1 and thus transiently enhances the coupling between the donor and acceptor states.

It is worth pointing out that the electron quantum dynamics performed keeping the nuclei fixed does not show electron injection on a few picosecods time scale even when geometries with α values outside the 70°−110° range extracted from the previous trajectory are used (as shown in Figure S2 in the Supporting Information for the initial geometry, $\alpha \approx 50°$). This indicates that ET is not solely promoted by a proper value of α but instead requires the coupling with other specific vibrational modes.[43] To identify those, we use the same nuclear trajectory to perform an EQD starting from the molecular configuration at 890 fs with α = 123° (Figure 2, just before the second shaded region). The results are presented in Figure 3b. Initially, while α > 110°, a limited injection (5%) is observed within the first ~50 fs. This transient is followed by a plateau up to ~230 fs,

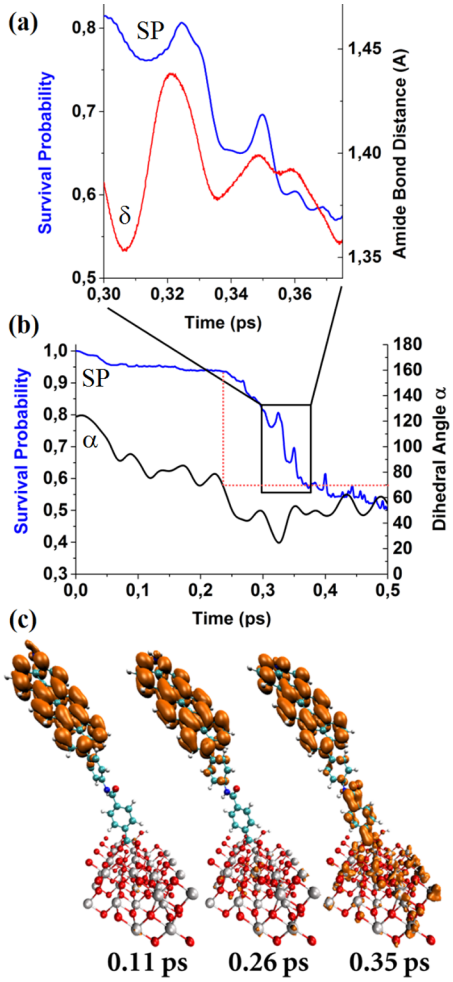

Figure 3. (a) Comparison between the survival probability (SP, blue line) oscillations and the amide bond (C−N) distance (δ, red line) along the EQD. (b) Comparison between the electron injection profile (SP, blue line) and the variation of the dihedral angle (α, black line) along the EQD simulation for the T-AM-TiO_2 system. The red dotted lines correlate the starting of the electron injection with the decrease in α below 70°. (c) Snapshots extracted along the EQD trajectory representing the electron wavepacket traveling through the bridge.

corresponding to the period during which 70° < α < 110°. Then, ET toward the TiO_2 is resumed by the decrease in α below the 70° threshold (red dotted lines in Figure 3b) and is characterized by electron density fluctuations with a period of ~30 fs (Figure 3b, black rectangle). The Fourier analysis of these rapid fluctuations gives a broad peak centered at ~1250 cm^{-1} (see Table 1a).

In Figure 3a it is shown that the oscillations characteristic of the electron injection (SP, blue line) are highly correlated with the variation of the amide bond distance N−C (δ, red line). A normal-mode analysis of the AM bridge shows that the N−C bond length is modulated by the normal modes ω_1 (1090 cm^{-1}) and ω_2 (1226 cm^{-1}) reported in Table 1. In fact, as described in Table 1b, these modes involve mostly the variation of the γ, δ, and ε bonds localized at the interface between the ED and EA orbitals (Table 1, Movies 2 and 3 in Supporting Information).

The energy fluctuations of these two orbitals are represented in Figure S4 of Supporting Information for a segment of the MD trajectory (0.1 to 0.4 ps), characteristic of the whole

DOI: 10.1021/acs.jpclett.5b00876
J. Phys. Chem. Lett. 2015, 6, 2393−2398

Table 1. (a) Frequencies of Relevant Normal Modes of the AM bridge (ω_1 and ω_2) Compared with the Frequency Obtained from the Fourier Analysis of the Electron Injection Oscillations along the EQD Trajectory and (b) Graphic Representation of the γ, δ, and ε Bond Distance Variations Associated to the Normal Modes ω_1 and ω_2[a]

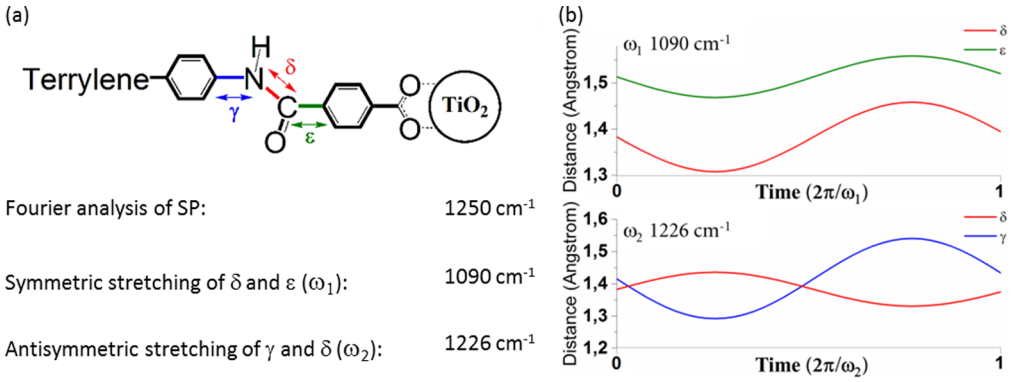

[a] γ, δ, and ε are the three bonds showing the major contribution to the normal modes ω_1 and ω_2.

simulation. The energies of EA and ED constantly cross each other, oscillating with distinctive frequencies of 1100 and 1235 cm^{-1}, respectively. The remarkable similarity between these two values and the frequencies of the normal modes ω_1 (1090 cm^{-1}) and ω_2 (1226 cm^{-1}) strongly indicates the influence of these particular vibrations on the energies of the electron donor and acceptor states. Overall, these results underline the importance of these specific nuclear vibrations in driving the electron injection. Similar evidence of vibronic coupling effects has been recently reported for different organic supramolecular complexes.[28,30,44]

Quantum coherent conversion from an excitonic state to a charge-transfer state requires that the two states partially occupy the same volume and that their energy levels are close enough to be coherently coupled by vibrational modes.[31−33,45−47] In the system discussed here, the two states involved in the electron transfer are associated with orbitals that initially are sufficiently close in energy but spatially separated. Thermal motion brings a conformational change (variation of α) that makes them partially occupy the same molecular region. Under this condition the two states can be coherently coupled by the fast vibrational modes localized at their interface, thus allowing the propagation of the electronic wavepacket by a convergence of electronic and nuclear dynamics.

A visual representation of the electron wavepacket propagating across the system is reported in Figure 3c and Movie 1 of Supporting Information. These snapshots clearly show how the wavepacket propagates through a channel, which is opened as a result of the Ph1 rotation. The snapshot at 0.35 ps clearly shows that the wavepacket can be described as a superposition of the corresponding ED and EA states, shown in Figure S3 in the Supporting Information. This demonstrates that the electron transfer is proceeding gradually from the ED state to the EA state, rather than hopping instantaneously.

In summary, the ET in T-AM-TiO_2 is driven by a strong coupling between the electron dynamics and specific nuclear vibrational modes. We have shown that the slow rotation of the bridge with respect to the antenna opens a preferential channel for the ET by changing the localization of the donor and acceptor states. When the channel is open, the charge can move across the bridge from the electron donor to the acceptor state driven by the bridge vibrational modes that induce the energy crossing and coupling of these two states.

These results underline the importance of including the nuclear dynamics for a proper description of the electron injection. Moreover we have verified the rectification properties of the AM bridge as part of a chromophore for a DSSC. The vibrational modes identified through the analysis of the correlation between nuclear and electron dynamics provide possible strategies for accelerating the electron injection process: we propose that structural modifications of the AM bridge preventing large rotations of the Ph1 ring could result in an increased efficiency.

■ ASSOCIATED CONTENT

Supporting Information

Technical details of the extended Hückel parameters optimization procedure. Quantum dynamics propagation of the hole and electron wave packets. DOS of a bare anatase surface. Comparison between DFT/B3LYP and EH optimized molecular orbitals for the isolated dye. Test on geometrical relaxation in the excited state. Electron and hole time-dependent survival probability profiles of the T-AM-TiO_2 system at fixed nuclear coordinates. Localization of the electron donor and electron acceptor states along the T-AM-TiO_2 MD trajectory. Electron donor and electron acceptor orbital energies along a portion of the EQD simulation. Test on T-Stilbene-TiO_2. Movie 1: Electron injection. Movies 2 and 3: normal modes ω_1 and ω_2. The Supporting Information is available free of charge on the ACS Publications website at DOI: 10.1021/acs.jpclett.5b00876.

■ AUTHOR INFORMATION

Corresponding Author

*E-mail: f.buda@chem.leidenuniv.nl.

Notes

The authors declare no competing financial interest.

■ ACKNOWLEDGMENTS

The use of supercomputer facilities was sponsored by NWO Physical Sciences, with financial support from The Netherlands Organization for Scientific Research (NWO). We acknowledge the use of the PRACE-3IP project (FP7 RI-312763) resources at ICM (IBM Power 7 based in Poland). This research is financed by the NWO-ECHO project number 713.011.002. V.S.B. acknowledges supercomputer time from NERSC and financial support as part of the Argonne-Northwestern Solar

DOI: 10.1021/acs.jpclett.5b00876
J. Phys. Chem. Lett. 2015, 6, 2393−2398

Energy Research (ANSER) Center, an Energy Frontier Research Center funded by the U.S. Department of Energy, Office of Science, Office of Basic Energy Sciences under Award Number DE-SC0001059.

REFERENCES

(1) O'Regan, B.; Grätzel, M. A Low-Cost, High-Efficiency Solar Cell Based on Dye-Sensitized Colloidal TiO2 Films. *Nature* **1991**, *353*, 737−740.
(2) Duncan, W. R.; Craig, C. F.; Prezhdo, O. V. Time-Domain Ab Initio Study of Charge Relaxation and Recombination in Dye-Sensitized TiO2. *J. Am. Chem. Soc.* **2007**, *129*, 8528−8543.
(3) Listorti, A.; O'Regan, B.; Durrant, J. R. Electron Transfer Dynamics in Dye-Sensitized Solar Cells. *Chem. Mater.* **2011**, *23*, 3381−3399.
(4) Nattestad, A.; Mozer, A. J.; Fischer, M. K. R.; Cheng, Y.-B.; Mishra, A.; Bäuerle, P.; Bach, U. Highly Efficient Photocathodes for Dye-Sensitized Tandem Solar Cells. *Nat. Mater.* **2010**, *9*, 31−35.
(5) Zhou, N.; Lin, H.; Lou, S. J.; Yu, X.; Guo, P.; Manley, E. F.; Loser, S.; Hartnett, P.; Huang, H.; Wasielewski, M. R.; et al. Morphology-Performance Relationships in High-Efficiency All-Polymer Solar Cells. *Adv. Energy Mater.* **2014**, *4*, 1−8.
(6) Hagfeldt, A.; Boschloo, G.; Sun, L.; Kloo, L.; Pettersson, H. Dye-Sensitized Solar Cells. *Chem. Rev.* **2010**, *110*, 6595−6663.
(7) Monti, A.; de Groot, H. J. M.; Buda, F. In-Silico Design of a Donor−Antenna−Acceptor Supramolecular Complex for Photo-induced Charge Separation. *J. Phys. Chem. C* **2014**, *118*, 15600−15609.
(8) Haid, S.; Marszalek, M.; Mishra, A.; Wielopolski, M.; Teuscher, J.; Moser, J.-E.; Humphry-Baker, R.; Zakeeruddin, S. M.; Grätzel, M.; Bäuerle, P. Significant Improvement of Dye-Sensitized Solar Cell Performance by Small Structural Modification in π-Conjugated Donor−Acceptor Dyes. *Adv. Funct. Mater.* **2012**, *22*, 1291−1302.
(9) Caprasecca, S.; Mennucci, B. Excitation Energy Transfer in Donor-Bridge-Acceptor Systems: A Combined Quantum-Mechanical/Classical Analysis of the Role of the Bridge and the Solvent. *J. Phys. Chem. A* **2014**, *118*, 6484−6491.
(10) Ma, W.; Jiao, Y.; Meng, S. Modeling Charge Recombination in Dye-Sensitized Solar Cells Using First-Principles Electron Dynamics: Effects of Structural Modification. *Phys. Chem. Chem. Phys.* **2013**, *15*, 17187−17194.
(11) Ambrosio, F.; Martsinovich, N.; Troisi, A. What Is the Best Anchoring Group for a Dye in a Dye-Sensitized Solar Cell? *J. Phys. Chem. Lett.* **2012**, *3*, 1531−1535.
(12) Koops, S. E.; O'Regan, B. C.; Barnes, P. R. F.; Durrant, J. R. Parameters Influencing the Efficiency of Electron Injection in Dye-Sensitized Solar Cells. *J. Am. Chem. Soc.* **2009**, *131*, 4808−4818.
(13) Meng, S.; Kaxiras, E. Electron and Hole Dynamics in Dye-Sensitized Solar Cells: Influencing Factors and Systematic Trends. *Nano Lett.* **2010**, *10*, 1238−1247.
(14) De Angelis, F. Modeling Materials and Processes in Hybrid/Organic Photovoltaics: From Dye-Sensitized to Perovskite Solar Cells. *Acc. Chem. Res.* **2014**, *47*, 3349−3360.
(15) De Angelis, F.; Fantacci, S.; Selloni, A.; Nazeeruddin, M. K.; Grätzel, M. Time-Dependent Density Functional Theory Investigations on the Excited States of Ru(II)-Dye-Sensitized TiO2 Nanoparticles: The Role of Sensitizer Protonation. *J. Am. Chem. Soc.* **2007**, *129*, 14156−14157.
(16) Nieto-Pescador, J.; Abraham, B.; Gundlach, L. Photoinduced Ultrafast Heterogeneous Electron Transfer at Molecule−Semiconductor Interfaces. *J. Phys. Chem. Lett.* **2014**, *5*, 3498−3507.
(17) Zhu, H.; Yang, Y.; Hyeon-Deuk, K.; Califano, M.; Song, N.; Wang, Y.; Zhang, W.; Prezhdo, O. V.; Lian, T. Auger-Assisted Electron Transfer from Photoexcited Semiconductor Quantum Dots. *Nano Lett.* **2014**, *14*, 1263−1269.
(18) Akimov, A. V.; Neukirch, A. J.; Prezhdo, O. V. Theoretical Insights into Photoinduced Charge Transfer and Catalysis at Oxide Interfaces. *Chem. Rev.* **2013**, *113*, 4496−4565.
(19) Akimov, A. V.; Prezhdo, O. V. Nonadiabatic Dynamics of Charge Transfer and Singlet Fission at the Pentacene/C $_{60}$ Interface. *J. Am. Chem. Soc.* **2014**, *136*, 1599−1608.
(20) Tafen, D. N.; Long, R.; Prezhdo, O. V. Dimensionality of Nanoscale TiO_2 Determines the Mechanism of Photoinduced Electron Injection from a CdSe Nanoparticle. *Nano Lett.* **2014**, *14*, 1790−1796.
(21) Long, R.; English, N. J.; Prezhdo, O. V. Minimizing Electron−Hole Recombination on TiO2 Sensitized with PbSe Quantum Dots: Time-Domain Ab Initio Analysis. *J. Phys. Chem. Lett.* **2014**, *5*, 2941−2946.
(22) Aviram, A.; Ratner, M. A. Molecular Rectifiers. *Chem. Phys. Lett.* **1974**, *29*, 277−283.
(23) Ding, W.; Negre, C. F. A.; Vogt, L.; Batista, V. S. Single Molecule Rectification Induced by the Asymmetry of a Single Frontier Orbital. *J. Chem. Theory Comput.* **2014**, *10*, 3393−3400.
(24) Ding, W.; Negre, C. F. A.; Palma, J. L.; Durrell, A. C.; Allen, L. J.; Young, K. J.; Milot, R. L.; Schmuttenmaer, C. A.; Brudvig, G. W.; Crabtree, R. H.; et al. Linker Rectifiers for Covalent Attachment of Transition-Metal Catalysts to Metal-Oxide Surfaces. *ChemPhysChem* **2014**, *15*, 1138−1147.
(25) Fleury, L.; Zumbusch, A.; Orrit, M.; Brown, R.; Bernard, J. Spectral Diffusion and Individual Two-Level Systems Probed by Fluorescence of Single Terrylene Molecules in a Polyethylene Matrix. *J. Lumin.* **1993**, *56*, 15−28.
(26) Harms, G. S.; Irngartinger, T.; Reiss, D.; Renn, A.; Wild, U. P. Fluorescence Lifetimes of Terrylene in Solid Matrices. *Chem. Phys. Lett.* **1999**, *313*, 533−538.
(27) Edvinsson, T.; Pschirer, N.; Schöneboom, J.; Eickemeyer, F.; Boschloo, G.; Hagfeldt, A. Photoinduced Electron Transfer from a Terrylene Dye to TiO2: Quantification of Band Edge Shift Effects. *Chem. Phys.* **2009**, *357*, 124−131.
(28) Andrea Rozzi, C.; Maria Falke, S.; Spallanzani, N.; Rubio, A.; Molinari, E.; Brida, D.; Maiuri, M.; Cerullo, G.; Schramm, H.; Christoffers, J.; et al. Quantum Coherence Controls the Charge Separation in a Prototypical Artificial Light-Harvesting System. *Nat. Commun.* **2013**, *4*, 1602.
(29) Chapman, C. T.; Liang, W.; Li, X. Ultrafast Coherent Electron−Hole Separation Dynamics in a Fullerene Derivative. *J. Phys. Chem. Lett.* **2011**, *2*, 1189−1192.
(30) Falke, S. M.; Rozzi, C. A.; Brida, D.; Maiuri, M.; Amato, M.; Sommer, E.; Sio, A. D.; Rubio, A.; Cerullo, G.; Molinari, E.; et al. Coherent Ultrafast Charge Transfer in an Organic Photovoltaic Blend. *Science* **2014**, *344*, 1001−1005.
(31) Romero, E.; Augulis, R.; Novoderezhkin, V. I.; Ferretti, M.; Thieme, J.; Zigmantas, D.; van Grondelle, R. Quantum Coherence in Photosynthesis for Efficient Solar-Energy Conversion. *Nat. Phys.* **2014**, *10*, 676−682.
(32) Chin, A. W.; Prior, J.; Rosenbach, R.; Caycedo-Soler, F.; Huelga, S. F.; Plenio, M. B. The Role of Non-Equilibrium Vibrational Structures in Electronic Coherence and Recoherence in Pigment-Protein Complexes. *Nat. Phys.* **2013**, *9*, 113−118.
(33) Fuller, F. D.; Pan, J.; Gelzinis, A.; Butkus, V.; Senlik, S. S.; Wilcox, D. E.; Yocum, C. F.; Valkunas, L.; Abramavicius, D.; Ogilvie, J. P. Vibronic Coherence in Oxygenic Photosynthesis. *Nat. Chem.* **2014**, *6*, 706−711.
(34) Hayes, D.; Griffin, G. B.; Engel, G. S. Engineering Coherence among Excited States in Synthetic Heterodimer Systems. *Science* **2013**, *340*, 1431−1434.
(35) Hoffmann, R. An Extended Hückel Theory. I. Hydrocarbons. *J. Chem. Phys.* **1963**, *39*, 1397−1412.
(36) Becke, A. D. Density-functional Thermochemistry. III. The Role of Exact Exchange. *J. Chem. Phys.* **1993**, *98*, 5648−5652.
(37) Lee, C.; Yang, W.; Parr, R. G. Development of the Colle-Salvetti Correlation-Energy Formula into a Functional of the Electron Density. *Phys. Rev. B* **1988**, *37*, 785−789.
(38) Rego, L. G. C.; Hames, B. C.; Mazon, K. T.; Joswig, J.-O. Intramolecular Polarization Induces Electron−Hole Charge Separation in Light-Harvesting Molecular Triads. *J. Phys. Chem. C* **2014**, *118*, 126−134.

DOI: 10.1021/acs.jpclett.5b00876
J. Phys. Chem. Lett. 2015, 6, 2393−2398

(39) Hoff, D. A.; da Silva, R.; Rego, L. G. C. Coupled Electron−Hole Quantum Dynamics on D−π−A Dye-Sensitized TiO2 Semiconductors. *J. Phys. Chem. C* **2012**, *116*, 21169−21178.
(40) *CPMD*, Copyright IBM Corp 1990−2008, Copyright MPI für Festkörperforschung Stuttgart 1997−2001. http://www.cpmd.org/.
(41) Olbrich, C.; Strümpfer, J.; Schulten, K.; Kleinekathöfer, U. Theory and Simulation of the Environmental Effects on FMO Electronic Transitions. *J. Phys. Chem. Lett.* **2011**, *2*, 1771−1776.
(42) Akimov, A. V.; Prezhdo, O. V. Persistent Electronic Coherence Despite Rapid Loss of Electron−Nuclear Correlation. *J. Phys. Chem. Lett.* **2013**, *4*, 3857−3864.
(43) Jiao, Y.; Ding, Z.; Meng, S. Atomistic Mechanism of Charge Separation upon Photoexcitation at the Dye−semiconductor Interface for Photovoltaic Applications. *Phys. Chem. Chem. Phys.* **2011**, *13*, 13196−13201.
(44) Eisenmayer, T. J.; Buda, F. Real-Time Simulations of Photoinduced Coherent Charge Transfer and Proton-Coupled Electron Transfer. *ChemPhysChem* **2014**, *15*, 3258−3263.
(45) Eisenmayer, T. J.; Lasave, J. A.; Monti, A.; de Groot, H. J. M.; Buda, F. Proton Displacements Coupled to Primary Electron Transfer in the Rhodobacter Sphaeroides Reaction Center. *J. Phys. Chem. B* **2013**, *117*, 11162−11168.
(46) Eisenmayer, T. J.; de Groot, H. J. M.; van de Wetering, E.; Neugebauer, J.; Buda, F. Mechanism and Reaction Coordinate of Directional Charge Separation in Bacterial Reaction Centers. *J. Phys. Chem. Lett.* **2012**, *3*, 694−697.
(47) Purchase, R. L.; de Groot, H. J. M. Biosolar Cells: Global Artificial Photosynthesis Needs Responsive Matrices with Quantum Coherent Kinetic Control for High Yield. *Interface Focus* **2015**, *5*, 20150014.

DOI: 10.1021/acs.jpclett.5b00876
J. Phys. Chem. Lett. 2015, 6, 2393−2398